MIR: A Mirror-Based Intermediate Reflector to Enhance Received Power in Free-Space Optical Communication Systems

Rui-Peng Li[1,2], Ya-Tian Li[1(✉)], Shi-Jie Gao[1,2], Tian-Wen Geng[1], Kai-Nan Yao[1,2], and Li-Mei Yin[1]

[1] Changchun Institute of Optics, Fine Mechanics and Physics, Chinese Academy of Sciences, Changchun 130033, China
yt_li@ciomp.ac.cn

[2] University of Chinese Academy of Sciences, Beijing 100049, China

Abstract. Free space optics (FSO) can achieve higher throughput due to a more concentrated energy by narrower divergence angle, compared with radio frequency (RF) communications. However, the receiver still cannot fully utilize all of the beam power, since the receiving aperture is always much smaller than the spot size at the receiving end. To capitalize on wasted power, we propose to add a Mirror-based Intermediate Reflector (MIR) in an FSO systems inspired by intelligent reflective surfaces, where the MIR can reflect part of the original lost energy to the receiving end. Based on geometric optics, the placement rules of the MIR are first obtained, where there are four criteria for the location and the angle. We further derive the expressions by regional integration method to quantify the power gain introduced by MIR. The derivation considers whether the reflected beams of the MIR all satisfy the case of incidence on the receiving target surface at an angle smaller than the field of view, and therefore the discussion is developed in two cases. Simulations show the feasibility of MIR, where the power gain is quantitatively illustrated. The results show that the reflection scheme can improve the received power gain, which provides a realizable approach to enhance the availability of FSO.

Keywords: Free space optics · Power gain · Intelligent reflective surfaces

This work is supported by the National Natural Science Foundation of China (NO. 62101527), Science and Technology Development Program of Jilin Province(20210401162YY), Chinese Academy of Sciences Key Project (YZQT024).

H.-H. Chen and W. Meng (Eds.): WiSATS 2024, LNICST 606, pp. 343–355, 2025.
https://doi.org/10.1007/978-3-031-86203-8_27

1 Introduction

1.1 Background

Free space optics (FSO), which has gained tremendous attention due to its high speed, high bandwidth, low latency, and high security characteristics, also can compensate for the crowded electromagnetic spectrum [1–3]. Compared to microwave, the properties of FSO communication system suggest that optical links are more suitable for linear unobstructed communication scenarios.

Various FSO links have been successfully demonstrated. Since 1994, when the National Institute of Information and Communication Technology (NICT) conducted the first star-ground laser communication between the Japanese Engineering Test Satellite-VI and a ground station, a large number of laser star-ground and interstellar laser communication test links have been consistently explored in terms of communication rates, equipment miniaturization, and so on [4–6]. SpaceX's Starlink and Telesat aim to create FSO satellite crosslinks in their constellations to provide global broadband internet access [7]. NASA and MIT Lincoln Laboratory are developing a 200 Gbps optical communication system for an LEO CubeSat [8,11].

However, in FSO systems, in addition to unavoidable losses such as atmospheric turbulence and absorption/scattering losses [9,10], large divergence angles or long communication distances often result in the received beam spot being much larger than the received aperture. The receiving aperture is unable to capture the energy of the entire beam spot, resulting in a significant amount of wasted energy. This energy loss reduces the communication capacity, and if the communication capacity is to be maintained, the communication distance is reduced, thus affecting the efficiency and performance of the system.

1.2 Related Words

The primary approach to addressing these challenges is through relaying. While relaying can indeed extend communication distance and increase communication capacity, it also increases system complexity and the costs associated with use and maintenance [12,13].

Intelligent reflective surfaces (IRS) have attracted considerable attention because they can be used to modify radio frequency (RF) wireless channels to improve communication performance [14]. IRS adjusts the phase and direction of the reflected signal through the reflection unit, which has low power consumption and simple structure. However, relaying relies on a terminal that receives, processes the received signal and sends it out, with a complex structure and high energy consumption.

Inspired by the application of IRS in the RF domain, researchers have explored the use of reflective surfaces to improve FSO communication performance. Marzieh Najafi et al. proposed an IRS based FSO system to mitigate the line-of-sight (LOS) requirement of traditional FSO systems. They developed a statistical channel model to assess the impact of reflective surface physical parameters on FSO channels. Simulation results validated the effectiveness

of this model for typical surface dimensions [15,16]. Haibo Wang et al. oriented point-to-multipoint FSO communication scenarios, and analyzed the IRS in terms of control mode, power efficiency, and beam splitting. Both simulations and experiments verified the feasibility of the models and algorithms [17]. This all proves that reflective surfaces are effective in space optical communication systems.

1.3 Motivation and Contribution

However, previous studies have primarily focused on the reflection of the beam as a whole. To the best of the authors' knowledge, no research has yet explored how to harness the energy outside the main beam to achieve power gain. Therefore, this paper proposes to use the reflection principle to collect the energy outside the main beam in order to obtain power gain at the receiver. The main contributions are summarized as follows.

- We propose an Mirror-based Intermediate Reflector(MIR) model aiming at increasing the energy at the receiver and improving the energy utilization of the FSO communication system to achieve a low-cost, high-efficiency link.
- Based on geometrical optics, an effective reflection region is given as a criterion for MIR placement, which includes constraints on MIR position, angle and size.
- In order to quantitatively describe the power gain, we employ a form of area integration. The integration object is the intensity distribution of the Gaussian beam. The intersection of the effective reflection region and the MIR is used as the integration region.
- According to whether the reflected beam of MIR can completely enter the receiving target surface, we divided the integration into two cases. And the derivation of Power gain is carried out separately.
- The power gain brought by MIR in the two cases is verified by simulation, which validates the theoretical significance and practical value of the scheme proposed in this paper.

The remainder of this paper is organized as follows. Section 2 demonstrates the system model. Section 3 analyzes the effective reflective region where the power gain for two cases. The simulation results are presented in Sect. 4. Finally, the conclusions of this paper are summarized in Sect. 5. For ease of reading, definitions of the main variables are summarized in Table 1.

2 System Model

A schematic diagram is given in Fig. 1(a). A beam from the transmitters with a divergence angle of θ travels a distance of L_1 to reach the receiving surface. The receiving aperture has a radius of r_0. Unlike conventional FSO systems, this paper considers an additional MIR, which can realize the power gain of the

Table 1. Definition of main variables.

Symbol	Definition
θ	Far-field divergence angle at the transmitter.
θ_{FOV}	Field-of-view angle at the receiver.
L_1	Communication distance.
r_0	Radius of the receiving surface.
r_{rm}	radius or half length of the finite large MIR model.
$(x_{\mathrm{rm}}, y_{\mathrm{rm}}, z_{\mathrm{rm}})$	Coordinates of the center point of the finite large MIR model.
φ_{rm}	Inclination of MIR (angle between MIR and Z axis).
$\vec{I}, \vec{R}$	Direction vectors of the incident and reflected beams on the MIR.
$\vec{P}$	the normal vector to the receiving target surface.
$J(x, y, z)$	Gaussian beam intensity distribution.
$\mathcal{G}_1$	Power gain when the reflected beams of the MIR can all enterthe receiving target surface.
$\mathcal{G}_2$	Power gain when a portion of the reflected beam of the MIR is not accessible to the receiving target surface.

receiver, and it has the advantages of simple structure, low cost, and wide applicability. As shown in Fig. 1(a), the beam received by the receiver consists of two parts. The orange section represents the main beam, which is the sole portion of light energy received by traditional FSO systems. In comparison, the red section denotes the beam reflected by the MIR. This reflected beam lies within the divergence angle but is outside the main beam. Based on the above description, the FSO downlink illustrated in Fig. 1(a) can be simplified to the theoretical system model shown in Fig. 1(b) by making the following assumptions:

- The transmitter emits a Gaussian beam.
- Since the communication distance is much larger than the Rayleigh distance, only the far-field divergence angle is considered. The focal point of the Gaussian beam is used as the origin of the coordinate system and the beam axis is the Z axis.
- The center of the receiving surface is located on the beam axis with coordinates $(0, 0, L_1)$.

According to the above assumptions, the system satisfies rotational symmetry on the beam axis. Points on a circle with the same distance from the center have the same properties at the same transmission distance. Therefore, any set of mutually perpendicular directions in the plane perpendicular to the Z axis are defined as the X axis and Y axis, respectively. The theoretical system model is schematically shown in Fig. 1(b).

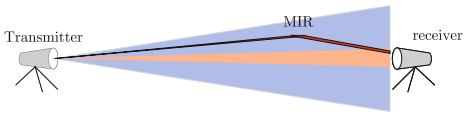

(a) Schematic diagram of the actual communication link.

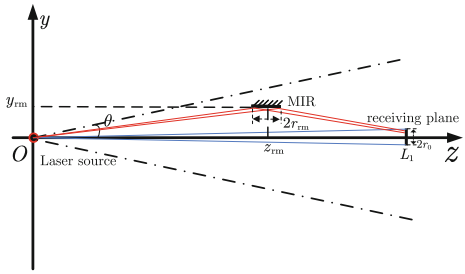

(b) Theoretical system model diagrams.

Fig. 1. Schematic diagram of the system model

Remark 1 lists the effective integration region based on the geometrical optics derivation, which is a constraint on the placement of the MIR.

Remark 1: The placement of MIR should follow the four criteria.

$$(1)\ \min\{\theta_{\mathrm{OL}}, \theta_{\mathrm{OR}}\} > \frac{r_0}{L_1}, \tag{1}$$

$$(2) z^2 < \cot^2\theta(x^2 + y^2), \tag{2}$$

$$(3)\ \frac{\vec{P}\cdot\vec{R}}{\left|\vec{P}\right|\left|\vec{R}\right|} > \cos\theta_{\mathrm{FOV}}, \tag{3}$$

$$(4)\ \left|\vec{I} + \frac{L_1 - z}{R_z}\vec{R}\right|^2 - L_1^2 \le r_0^2, \tag{4}$$

where (x, y, z) denotes the coordinates of any point on the MIR, θ_{OL} and θ_{OR} denotes the angle between the line connecting the edge point of MIR in the Z axis direction with the origin and the Z axis, θ_{FOV} denotes the field-of-view angle of the receiving surface, as shown in Fig. 2(a). $\vec{I}$ and $\vec{R}$ denote the direction vector of the MIR incident beam and the corresponding direction vector of the reflected beam, respectively. R_z is the z component of $\vec{R}$ and $\vec{P}$ is the unit normal vector of the receiving surface.

A further explanation of the above four criteria is shown below.

(1) The MIR should not block the main beam, and since the MIR is a plane reflector, this means that it is only necessary to require that the MIR does not block the main beam in the YOZ plane.

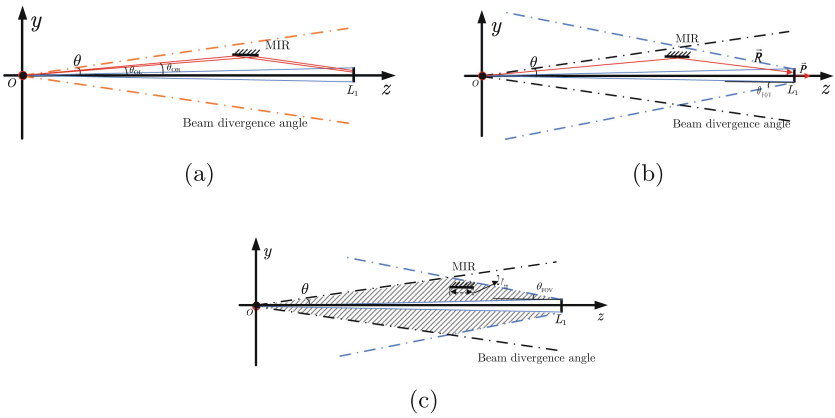

Fig. 2. Conditions that need to be met for the placement of the MIR. (*a*) shows a schematic diagram of criterion (1) versus criterion (2); (*b*) shows a schematic diagram of criterion (3) versus criterion (4); and (*c*) demonstrates the possible placement locations of MIR.

(2) To ensure effective reflected power gain, the MIR should be within the Gaussian divergence angle.
(3) The direction vector of the reflected beam via the MIR should satisfy the field-of-view requirement, meaning that the angle with the normal vector of the receiving target surface should be less than the field-of-view angle.
(4) Due to the translation invariant nature of the vectors, in addition to the requirement that the reflected beam meets the field of view requirements, it is also required that the reflected beam passes through the receiving target surface. This is determined by judging the distance between the intersection point of the reflected beam in the $z = L_1$ plane and the center of the receiving target surface.

The requirements of criterion (1) and criterion (2) are shown in Fig. 2(a), and the MIR reflected beam needs to be incident with the field of view requirements of the receiving surface (criterion (3)) into the receiving target surface (criterion (4)) as shown in Fig. 2(b). Figure Fig. 2(c), on the other hand, gives a visualization of the possible placement areas of a MIR. It is worth noting that the above conditions are sufficient but not necessary for the MIR placement location.

3 Theoretical Derivation of Power Gain

The region satisfying Remark 1 above is denoted as P_1, which is the effective reflection area, while the actual reflection region of the MIR is denoted as P_2. Therefore, depending on whether the MIR is fully contained in the effective reflective region, i.e., whether all reflected beams on the MIR can be incident on the receiving target surface at less than the field of view, there are two cases:

$P_2 \subset P_1$ and $P_2 \not\subset P_1$. The actual reflection region is $P_1 \cap P_2$, which is the integration region. Therefore, when $P_2 \subset P_1$ holds, the region of integration is $P_1 \cap P_2 = P_2$.

3.1 Integral Area Analysis

The equation $y - tan\varphi_{\mathrm{rm}}(z - z_{\mathrm{rm}}) - y_{\mathrm{rm}} = 0$, represents the plane in which the MIR is located. Where $(0, y_{\mathrm{rm}}, z_{\mathrm{rm}})$ is the point of the MIR in the YOZ plane, which is defined as the center coordinate of the MIR in this paper for the convenience of computation. The inclination of the MIR is denoted by φ_{rm}, which is the angle of the MIR with the Z axis, since the MIR is in a plane perpendicular to the YOZ plane.

Since both P_1 and P_2 are integrated in the beam propagation space, which is more complicated, so we project to the XOZ plane for integration.

Remark 2: The projection P_1' of the effective reflection region P_1 in the XOZ plane satisfies

$$(1)\frac{r_0}{L_1} \leq \frac{\sqrt{x^2 + (tan\varphi_{\mathrm{rm}} z_{\mathrm{rm}} + k)^2}}{z} \leq \tan\theta, \tag{5}$$

$$(2)x^2 < \tan^2\theta_{\mathrm{FOV}}\left[z + k\sin 2\varphi_{\mathrm{rm}}\right]^2 - \left[\tan\varphi_{\mathrm{rm}} z - k\cos 2\varphi_{\mathrm{rm}}\right]^2, \tag{6}$$

$$(3)\frac{x^2}{m_0} + \frac{(z - z_{\mathrm{c0}})^2}{n_0} \leq 1, \tag{7}$$

where k is equal to $y_{\mathrm{rm}} - \tan\varphi_{\mathrm{rm}} z_{\mathrm{rm}}$, whose geometrical significance is the intercept of the MIR on the Y axis. On the other hand, derivation from the above information leads to the parameters of Eq. (7) are as follows.

$$m_0 = \frac{r_0 k}{\sqrt{(L_1\tan\varphi_{\mathrm{rm}} + 2k)^2 - r_0^2}}, \tag{8}$$

$$n_0 = \frac{\left(\sin 2\varphi_{\mathrm{rm}} + 1 - \tan^2\varphi_{\mathrm{rm}}\right) L_1 + \left(2\sin 2\varphi_{\mathrm{rm}} - \tan\varphi_{\mathrm{rm}}\right) k}{(L_1\tan\varphi_{\mathrm{rm}} + 2k)^2 - r_0^2} r_0 k, \tag{9}$$

$$z_{\mathrm{c0}} = \frac{(L_1\tan\varphi_{\mathrm{rm}} + 2k)\left(L_1 - L_1\tan^2\varphi_{\mathrm{rm}} + k\tan\varphi_{\mathrm{rm}}\right) + r_0^2\sin 2\varphi_{\mathrm{rm}}}{(L_1\tan\varphi_{\mathrm{rm}} + 2k)^2 - r_0^2} k, \tag{10}$$

where criterion (1) is the first two requirements in Remark 1, and any point on the MIR satisfies that it does not block the main beam and is within the divergence angle, as is evident in its expression. In general, criterion (2) and criterion (3) are tighter requirements, so those points that satisfy criterion (2) and criterion (3) satisfy criterion (1).

Remark 3: The projection of the MIR onto the XOZ plane is denoted as P_2'.

$$\frac{x^2}{r_{\mathrm{rm}}^2} + \frac{(z - z_{\mathrm{rm}})^2}{(r_{\mathrm{rm}}\cos\varphi_{\mathrm{rm}})^2} \leq 1 \tag{11}$$

according to the model parameters, the projections of P_1 and P_2 in the XOZ plane are P_1' and P_2', respectively, and analytic expressions are given. Under the same condition, $P_2' \subset P_1'$ holds when $P_2 \subset P_1$. Similarly, $P_2' \not\subset P_1'$ when $P_2 \not\subset P_1$ holds under the same condition. Thus, the two cases to be analyzed can be equivalently expressed as $P_2' \subset P_1'$ and $P_2' \not\subset P_1'$. At this point, we correspond P_1 and P_2 to the P_1' and P_2' mentioned in Remark 2 and Remark 3, respectively. The obtained P_1' and P_2' will guide the subsequent derivations.

3.2 Gain Analysis When $P_2 \subset P_1$

If all reflected beams from the MIR can enter the receiving target surface within the field of view, then it holds that $P_2 \subset P_1$, which also means that the MIR is entirely within the P_1 region. Consider a circular reflecting surface with a radius of r_{rm}, whose center coordinates are $(0, y_{\mathrm{rm}}, z_{\mathrm{rm}})$ and whose inclination angle is φ_{rm}.

Lemma 1: The light field integral of the actual reflection area of the MIR can be expressed as

$$\mathcal{I}_1 = \iint_{S_1} J\left(x, y, z\right) dS, \tag{12}$$

where the integration region is $S_1 = P_1 \cap P_2 = P_2$, and the Gaussian beam has the following intensity distribution.

$$J\left(x, y, z\right) = \frac{J_0^2}{\omega^2\left(z, \omega_0\right)} \exp\left(\frac{-2r^2}{\omega^2\left(z, \omega_0\right)}\right), \tag{13}$$

among them, ω_0 represents the beam waist radius, λ is the wavelength of light, and J_0 is the irradiance at the center of the optical beam waist. Furthermore, $\omega\left(z, \omega_0\right) = \omega_0\sqrt{1 + \left(z/z_R\right)^2}$ is the beam width at distance z, the Rayleigh distance is $z_R = \frac{\pi\omega_0^2}{\lambda}$, and the relationship between the beam waist radius and the far-field divergence angle is $\omega_0 = \frac{2\lambda}{\pi\theta}$. In addition, based on the communication distance L_1 and the radius of the receiving target surface r_{rm}, the main beam energy received by the receiving target surface may be expressed as $\mathcal{I}_0 = \frac{\pi}{2} J_0^2 \left[1 - \exp\left(-r_0^2 / w\left(L_1, \omega_0\right)\right)\right]$.

Lemma 2: Considering $\mathcal{I}_1$ as a surface integral, it can be projected onto the XOZ plane and expressed as

$$\mathcal{I}_2 = \iint_{S_2} J\left(x, \varphi(x, z), z\right) \sqrt{1 + \left(\varphi'_x\right)^2 + \left(\varphi'_z\right)^2} dx dz, \tag{14}$$

among them, $y = \varphi(x, z) = \tan\varphi_{\mathrm{rm}}(z - z_{\mathrm{rm}}) + y_{\mathrm{rm}}$ is the expression for the plane in which the MIR is located. So the integral area $S_2 = P_1' \cap P_2' = P_2'$. The energy gain is expressed as

$$\mathcal{G}_1 = 10\log_{10}\left(\frac{\mathcal{I}_0 + \mathcal{I}_2}{\mathcal{I}_0}\right) \tag{15}$$

3.3 Gain Analysis When $P_2 \not\subset P_1$

If there is a portion of the beam reflected by the MIR that cannot be incident on the receiving target surface at an angle less than the field of view, then $P_2 \not\subset P_1$. Consequently, the integration area is $P_1' \cap P_2'$.

Lemma 3: For the integration region $S_3 = P_1' \cap P_2'$, the energy gain is expressed as the following integral

$$\mathcal{I}_3 = \iint_{S_3} J\left(x, \varphi(x,z), z\right) \sqrt{1 + \left(\varphi'_x\right)^2 + \left(\varphi'_z\right)^2} dxdz. \tag{16}$$

Let the intersection points of P_2' and P_1' be z_1 and $z_2 (z_1 < z_2)$ respectively, and they can be determined by Eq. (11) and Eq. (7) when taking the equal sign. Then the above expression can be divided into three partial integrals according to the region of integration, $S_3 = S_3^{(1)} + S_3^{(2)} + S_3^{(3)}$. Denote the integrated function as $f(x,z)$, then $\mathcal{I}_3$ can be expressed as the following equation.

$$\mathcal{I}_3 = \iint_{S_3^{(1)}} f\left(x,z\right) dxdz + \iint_{S_3^{(2)}} f\left(x,z\right) dxdz + \iint_{S_3^{(3)}} f\left(x,z\right) dxdz \tag{17}$$

where the integration region $S_3^{(2)}$ satisfies Eq. (7), with the variable z taking values in (z_1, z_2). The integration regions $S_3^{(1)}$ and $S_3^{(3)}$ satisfy Eq. (11), where the variable z takes values within the ranges $(z_{\mathrm{rm}} - r_{\mathrm{rm}} \cos\varphi_{\mathrm{rm}}, z_1)$ and $(z_2, z_{\mathrm{rm}} + r_{\mathrm{rm}} \cos\varphi_{\mathrm{rm}})$, respectively. With the same MIR placement, as r_{rm} increases, the integration formula transitions from $\mathcal{I}_2$ to $\mathcal{I}_3$, with the boundary at $r_{\mathrm{rm\,max}} = m_0 \sqrt{1 - \frac{(z - z_{\mathrm{c0}})^2}{n_0^2}}$. The energy gain is expressed as

$$\mathcal{G}_2 = 10 \log_{10} \left(\frac{\mathcal{I}_0 + \mathcal{I}_3}{\mathcal{I}_0} \right) \tag{18}$$

4 Simulation Results

In this section, we will calculate and analyze the integration region and power gain results. We will illustrate the integration regions for the cases $P_2 \subset P_1$ and $P_2 \not\subset P_1$, as well as the variations in power gain with changes in the MIR position and radius. Since the P_1 region is determined by the position and inclination of the MIR, and the placement region of the MIR depends on the P_1 region, we will provide the upper and lower bounds for the finite placement region of the MIR in different scenarios. This analysis aims to rigorously elucidate the dependencies between these parameters.

4.1 Integral Area

In this subsection, the results of the simulation calculations in the integration region are given. In the subsequent simulation, the default value of the communication distance L_1 is set to 1000 m, the far-field divergence angle θ is set to

1 mrad, the optical wavelength λ is selected to be 1550 nm, and the radius and field-of-view of the receiving target surface are set to be 0.2 m and 0.9 mrad, respectively. Based on the above parameter settings, Fig. 3 demonstrates the integration region corresponding to the two cases of $P_2 \subset P_1$ and $P_2 \not\subset P_1$. Where the coordinates of the center point of the MIR are $(0, 700\,\text{m}, 0.25\,\text{m})$, the inclination angle is 0.17 mrad, and the radius are 0.23 m and 0.11 m, respectively.

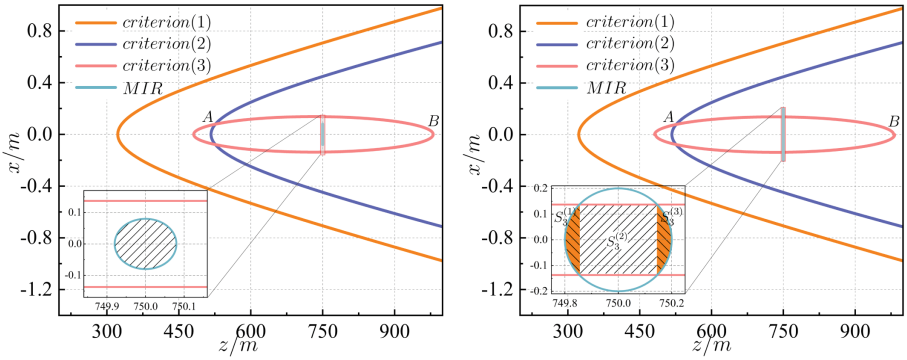

Fig. 3. The relationship between P_1' and P_2'.

In long-distance communications, the spot on the received target surface is significantly larger than the diameter of the received target surface, which ensures that the requirements of MIR within the divergence angle and without blocking the main beam are easily met. Figure 3 shows the projection of the plane where the MIR is located. The blue curve indicates the requirement that the reflected beam be less than the field of view for incidence, and any reflected beam on the MIR beyond this curve is greater than the field of view. The pink curve, on the other hand, represents the beam reflected by the MIR into the receiving target surface, even though part of the beam has an angle of incidence greater than the field of view.

The intersection of the criterion (2) and criterion (3) curves is denoted as point A, and the rightmost point of the criterion (3) curve is denoted as point B. Therefore, MIR should be located between point A and point B, with their respective z coordinates noted as $inf(z_{\text{rm}})$ and $sup(z_{\text{rm}})$. Since the reflected beam in the region smaller than $inf(z_{\text{rm}})$ needs to be incident close to the field of view, it is highly inefficient and thus not considered. Additionally, the radius of the MIR should not be significantly larger than the receiving surface based on practical application scenarios. Therefore, it is reasonable to consider only the criterion(3) limitations when $P_2 \not\subset P_1$.

4.2 Power Gain

This subsection gives the relationship between power gain and the position of the MIR. Considering the different positions of the MIR, the range of choices for the inclination is not the same, the MIR inclination angle used for the simulations in this section is $\varphi_{\mathrm{rm}} = \frac{y_{\mathrm{rm}}}{2z_{\mathrm{rm}}} - \frac{1}{4}\theta_{\mathrm{FOV}}$. Figure 4 presents the trend of the gain with z_{rm} under the condition of $y_{\mathrm{rm}} = 0.25$ m. The upper and lower bounds of z_{rm} at the corresponding position and the current value of z_{rm} are shown, illustrating the reasonableness of the selected z_{rm} values. In Fig. 4(a) and Fig. 4(b), the radius R_{rm} is set to 0.08 m and 0.20 m, respectively, to illustrate the gain in the cases of $P_2 \subset P_1$ and$P_2 \not\subset P_1$, and to quantitatively compare the effect of the radius at the same position on the gain.

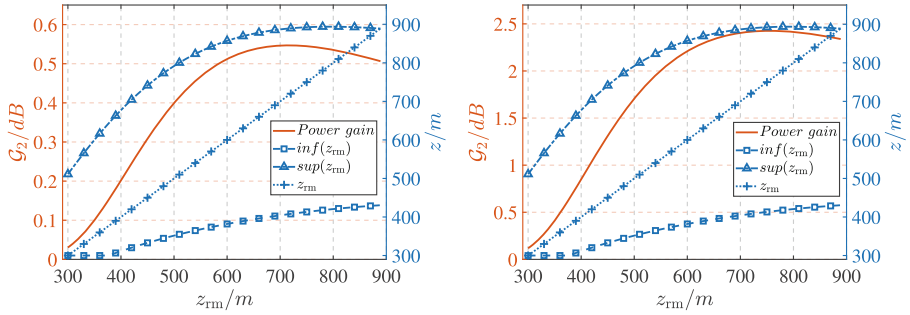

(a) $P_2 \subset P_1,\ r_{\mathrm{rm}} = 0.08\mathrm{m}$ (b) $P_2 \not\subset P_1,\ r_{\mathrm{rm}} = 0.20\mathrm{m}$

Fig. 4. Trend of gain with z_{rm} for different radius r_{rm} values and upper and lower bounds of the range in which MIR can be placed.

Figure 5 illustrates the variation of power gain with y_{rm} when $z_{\mathrm{rm}} = 680\mathrm{m}$ and $r_{\mathrm{rm}} = 0.11\mathrm{m}$. As y_{rm} increases, the power gain decreases. Where $r_{\mathrm{rm}} > r_{\mathrm{rm\ max}}$ when y_{rm} is greater than 0.269m, overshooting from $P_2 \not\subset P_1$ to $P_2 \subset P_1$. On the other hand, it also shows that $\mathcal{G}_1$ and $\mathcal{G}_2$ are continuous on the boundary in the same case.

From Fig. 4, it can be seen that not the closer the transmitter and receiver to obtain the greater the energy gain, can obtain the maximum gain when the MIR is in the middle of the communication distance slightly close to the receiving end side. From Fig. 5, when the z coordinate of the MIR is determined, the closer to the beam axis, the greater the gain. However, there is a limit to this proximity in order not to block the main beam. Obviously the maximum power gain that can be achieved is 0.7dB for $P_2 \subset P_1$ due to the small radius of the MIR, and then the maximum power gain can reach 2.4dB for $P_2 \not\subset P_1$. In practice, the suitable installation position should be determined according to the communication distance and the radius of the reflector. Taken together, the gain of $P_2 \not\subset P_1$ is greater than that of $P_2 \subset P_1$, but this will bring additional costs.

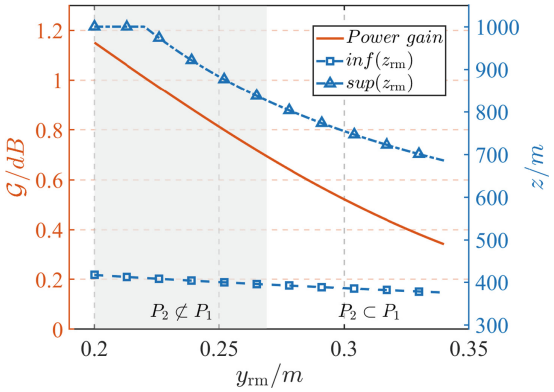

Fig. 5. The trend of gain with y_{rm} and the upper and lower bounds of the range in which MIR can be placed.

5 Conclusion

This paper proposes to utilize MIR to increase the received power gain in the FSO. Based on the principle of geometric optics, the MIR should satisfy the four basic criteria of not blocking the main beam, being within the divergence angle, the angle of the reflected beam being less than the field of view of the receiver, and the reflected beam being incident on the receiving target surface. Accordingly, the power gain is derived using area integration. Whether or not all the points on the MIR satisfy the four basic criteria is analyzed in two cases. Through simulation analysis, the MIR is placed slightly closer to the receiving side, close to the optical axis but not blocking the main beam to obtain a higher power gain. The incremental gain in the $P_2 \not\subset P_1$ case is up to 2.4 dB, which is higher than the incremental gain of 0.7 dB in the $P_2 \subset P_1$ case. However, the high gain at $P_2 \not\subset P_1$ is due to the large aperture MIR, and the best installation position and angle should be selected according to the position where the MIR can be installed, the aperture of the existing reflective surface and the communication distance. We will further explore the optimal placement and angle of the MIR and experimentally verify the power gain of the MIR in the future.

References

1. Al-Gailani, S.A., Salleh, M.F.M., Salem, A.A., et al.: A survey of free space optics (FSO) communication systems, links, and networks. IEEE Access **9**, 7353–7373 (2020)
2. Li, Y.T., Geng, T.W., Gao, S.J.: Likelihood based synchronization algorithms in optical pulse position modulation systems with photon-counting receivers. Opt. Express **30**(17), 31472–31485 (2022)
3. Trichili, A., Cox, M.A., Ooi, B.S., et al.: Roadmap to free space optics. J. Opt. Soc. Am. B **37**(11), A184–A201 (2020)

4. Boroson, D.M., Robinson, B.S., Murphy, D.V., et al.: Overview and results of the lunar laser communication demonstration. In: Proceedings of the SPIE 8971, Free-Space Laser Communication and Atmospheric Propagation XXVI, pp. 213–223 (2014)
5. Toyoshima, M., Leeb, W.R., Kunimori, H., et al.: Comparison of microwave and light wave communication systems in space applications. Opt. Eng. **46**(1), 015003-1–015003-7 (2007)
6. Akioka, M., Takenaka, H., Toyoshima, M., et al.: The NICT's new OGS for satellite laser communication and SOTA/SOCRATES experiment. In: Proceedings of the SpaceOps Conference (2016)
7. Del Portillo, I., Cameron, B.G., Crawley, E.F.: A technical comparison of three low earth orbit satellite constellation systems to provide global broadband. Acta Astronaut. **159**, 123–135 (2019)
8. Robinson, B.S., Boroson, D.M., Schieler, C.M., et al.: TeraByte InfraRed Delivery (TBIRD): a demonstration of large-volume direct-to-Earth data transfer from low-Earth orbit. In: Proceedings of the SPIE 10524, Free-Space Laser Communication and Atmospheric Propagation XXX, pp. 253–258 (2018)
9. Nistazakis, H.E., Tsiftsis, T.A., Tombras, G.S.: Performance analysis of free-space optical communication systems over atmospheric turbulence channels. IET Commun. **3**(8), 1402–1409 (2009)
10. Kaushal, H., Kaddoum, G.: Optical communication in space: challenges and mitigation techniques. IEEE Commun. Surveys Tuts. **19**(1), 57–96 (2016)
11. Schieler, C.M., Riesing, K.M., Horvath, A.J., et al.: 200 Gbps TBIRD CubeSat downlink: pre-flight test results. In: Proceedings of the SPIE 11993, Free-Space Laser Communications XXXIV, pp. 200–206 (2022)
12. Khalighi, M.A., Uysal, M.: Survey on free space optical communication: a communication theory perspective. IEEE Commun. Surveys Tuts. **16**(4), 2231–2258 (2014)
13. Qu, L., Xu, G., Zeng, Z., et al.: UAV-assisted RF/FSO relay system for space-air-ground integrated network: a performance analysis. IEEE Trans. Wireless Commun. **21**(8), 6211–6225 (2022)
14. Wu, Q., Zhang, R.: Intelligent reflecting surface enhanced wireless network via joint active and passive beamforming. IEEE Trans. Wireless Commun. **18**(11), 5394–5409 (2019)
15. Najafi, M., Schober, R.: Intelligent reflecting surfaces for free space optical communications. In: Proceedings of the 2019 IEEE Global Communications Conference (GLOBECOM), pp. 1–7 (2019)
16. Najafi, M., Schmauss, B., Schober, R.: Intelligent reflecting surfaces for free space optical communication systems. IEEE Trans. Commun. **69**(9), 6134–6151 (2021)
17. Wang, H., Zhang, Z., Zhu, B., et al.: Approaches to array-type optical IRSs: schemes and comparative analysis. J. Lightwave Technol. **40**(12), 3576–3591 (2022)